Relativistic multireference many-body perturbation-theory calculations of the magnetic-dipole and electric-quadrupole transition probabilities of ions in the silicon isoelectronic sequence

Yasuyuki Ishikawa and Marius Jonas Vilkas
Department of Chemistry, University of Puerto Rico, P.O. Box 23346, San Juan, Puerto Rico 00931-3346
(Received 1 November 2000; published 15 March 2001)

Relativistic multireference many-body perturbation theory is employed to calculate the energy spectra, magnetic-dipole, and electric-quadrupole transition probabilities of the lowest ^3P_J fine-structure states of ions in the silicon isoelectronic sequence. Theoretical lifetimes of the $^3P_{1,2}$ states are evaluated and compared with recent experiments.

DOI: 10.1103/PhysRevA.63.042506 PACS number(s): 31.15.Md, 31.30.Jv, 31.25.Jf, 32.70.Cs

I. INTRODUCTION

There has been considerable interest in the electronic transitions and radiative transition rates among multiplet states of open-shell ions [1–3]. Accurate estimates of radiative transition probabilities among multiplet states are an important source for successful experimental identification of the spectra of astrophysical and laboratory plasma. Probabilities of magnetic-dipole and electric-quadrupole transitions, in particular, are important in plasma diagnostics, but experimental determination of these quantities is difficult, and accurate theoretical estimates provide valuable information. A number of theoretical calculations on electric and magnetic multipole transition rates have been performed in recent years by various approximations, and it has become evident that accurate, correlated wave functions must be employed to evaluate the transition rates accurately [4–8].

Relativistic multiconfiguration Dirac-Fock (MCDF) self-consistent-field (SCF) calculations have been widely employed to calculate transition energies and transition rates. Relativistic MCDF SCF is effective in treating nondynamic correlation. It fails, however, to account for the bulk of dynamic correlation, and thus often fails to provide accurate transition energies, and semiempirical adjustment of computed transition rates is required to obtain agreement with experiment. For the electric-dipole forbidden transitions in high-Z ions, electric-quadrupole ($E2$) transition rates are dominant over magnetic-dipole ($M1$) rates. Accurate calculation of transition energies is necessary because $E2$ transition rates involve a fifth power dependence on transition energy. Thus, an accurate relativistic many-body algorithm must be brought to bear on the prediction of transition energies and transition rates [5–8]. One of the most advanced methods for treating many-electron systems is relativistic multireference Møller-Plesset perturbation theory (MR-MP) [9] based on multiconfiguration Dirac-Fock-Breit (MCDFB) SCF wave functions [10]. Relativistic MR-MP accounts for relativistic, nondynamic, and dynamical Dirac-Coulomb and Breit correlation energies and Lamb shift corrections in transition energy calculations. It can provide accurate transition energies and transition rates among multiplet states of atoms for a broad range of ionizations.

Recently, the intense $3s^2 3p^2\,{}^3P_2$-$^3P_1$ line in the visible spectrum of a siliconlike krypton ion, first observed in a tokamak fusion test plasma [11], was observed using an electron beam ion trap [12]. The lifetime of the $3s^2 3p^2\,{}^3P_2$ state was measured in three recent experiments [12–14]. The most recent determination [12], with a novel transmission grating spectrometer of higher speed and spectral resolution, deviates significantly from the previous two. In the present study, we employ recently developed relativistic MR-MP [9,15] to calculate the energy levels of the $3s^2 3p^2\,{}^3P_{0,1,2}$ fine-structure states, $M1$ and $E2$ transition probabilities among these levels, and the lifetimes of the $^3P_{1,2}$ states of ions in the silicon isoelectronic sequence. The theoretical lifetime of the $^3P_2$ state of a siliconlike krypton ion is compared with the three recent experimental results.

II. METHOD

A. Relativistic multireference many-body perturbation theory

The effective N-electron Hamiltonian (in atomic units) for the development of our relativistic MR-MP algorithm is taken to be the relativistic ''no-pair'' Dirac-Coulomb-Breit (DCB) Hamiltonian [16,17],

$$H_{\mathrm{DCB}}^{+}=\sum_i h_D(i)+\mathcal{L}_+\left(\sum_{i>j}\frac{1}{r_{ij}}+B_{ij}\right)\mathcal{L}_+ \tag{1}$$

with

$$B_{ij}=-\frac{1}{2}[\boldsymbol{\alpha}_i\cdot\boldsymbol{\alpha}_j+(\boldsymbol{\alpha}_i\cdot\mathbf{r}_{ij})(\boldsymbol{\alpha}_j\cdot\mathbf{r}_{ij})/r_{ij}^2]/r_{ij}\,. \tag{2}$$

Here $h_D(i)$ is the Dirac one-electron Hamiltonian. The DCB Hamiltonian is covariant to first order and increases the accuracy of calculated fine-structure splittings and inner-shell binding energies. Higher-order QED effects appear first in order α^3. The nucleus is modeled as a sphere of uniform proton charge distribution. $\mathcal{L}_+=L_+(1)L_+(1)\cdots L_+(1)$, where $L_+(1)$ is the projection operator onto the space $D^{(+)}$ spanned by the positive-energy eigenfunctions of the matrix Dirac-Fock-Breit (DFB) SCF equation [17,18]. $\mathcal{L}_+$ is the projection operator onto the positive-energy space $\mathfrak{D}^{(+)}$ spanned by the N-electron configuration-state functions (CFSs) constructed from the positive-energy eigenfunctions of the matrix DFB SCF. It takes into account the field-theoretic condition that the negative-energy states be filled. The eigenfunctions of the matrix DFB SCF equation clearly

separate into two discrete manifolds, $D^{(+)}$ and $D^{(-)}$, respectively, of positive- and negative-energy states. As a result, the positive-energy projection operators can be accommodated easily in many-body calculations. The formal conditions on the projection are automatically satisfied when only the positive-energy spinors are employed.

N-electron eigenfunctions of the no-pair DCB Hamiltonian are approximated by a linear combination of M configuration-state functions, $\{\Phi_I^{(+)}(\gamma_I\mathcal{J}\pi);I=1,2,\ldots,M\} \in \mathfrak{P}^{(+)}$, constructed from positive-energy eigenfunctions of the matrix MCDFB SCF equation [10],

$$\psi_K(\gamma_K\mathcal{J}\pi)=\sum_I^M C_{IK}\Phi_I^{(+)}(\gamma_I\mathcal{J}\pi). \tag{3}$$

The MCDFB SCF wave function $\psi_K(\gamma_K\mathcal{J}\pi)$ is an eigenfunction of the angular momentum and parity operators with total angular momentum $\mathcal{J}$ and parity π. γ denotes a set of quantum numbers other than $\mathcal{J}$ and π necessary to specify the state uniquely. The total DCB energy of the general MCDFB electronic state $\psi_K(\gamma_K\mathcal{J}\pi)$ can be expressed as

$$E^{\mathrm{MC}}(\gamma_K\mathcal{J}\pi)=\sum_{IJ}^{(+)} C_{IK}C_{JK} \times\langle\Phi_I^{(+)}(\gamma_I\mathcal{J}\pi)|H_{\mathrm{DCB}}^{+}|\Phi_J^{(+)}(\gamma_J\mathcal{J}\pi)\rangle. \tag{4}$$

Here, it is assumed that $\psi_K(\gamma_K\mathcal{J}\pi)$ and $\Phi_J^{(+)}(\gamma_J\mathcal{J}\pi)$ are normalized. Matrix MCDFB SCF calculations were performed to obtain a single set of spinors for all the ${}^{2S+1}L_{\mathcal{J}}$ fine-structure states by optimizing the $\mathcal{J}$-averaged MC energies, providing the same radial spinors for the different $\mathcal{J}$ states [9],

$$E_{\mathcal{J}\text{-av}}^{\mathrm{MC}}=\sum_{\mathcal{J}}\frac{(2\mathcal{J}+1)}{\sum_{\mathcal{J}'}(2\mathcal{J}'+1)}E^{\mathrm{MC}}(\gamma_K\mathcal{J}\pi), \tag{5}$$

where summation $\mathcal{J}$ and $\mathcal{J}'$ runs over a set of ${}^{2S+1}L_{\mathcal{J}}$ ($\mathcal{J}=|L-S|,\ldots,|L+S|$) fine-structure states. S and L are the spin and orbital angular momentum quantum numbers. To remove the arbitrariness of the matrix MCDFB SCF spinors and density weighting [19,20], the canonical SCF spinors are transformed into natural spinors for subsequent perturbation calculations.

The no-pair DCB Hamiltonian H_{DCB}^{+} is decomposed into two parts, unperturbed Hamiltonian H_0 and perturbation V, following Møller and Plesset [19–21],

$$H_{\mathrm{DCB}}^{+}=H_0+V=\sum_i^N F_{\mathrm{av}}(i)+V, \tag{6}$$

where the unperturbed model Hamiltonian H_0 is a sum of average DF operators F_{av} [19]. The application of Rayleigh-Schrödinger perturbation theory provides order-by-order expressions of the perturbation series for the zero-order state approximated by $|\psi_K(\gamma_K\mathcal{J}\pi)\rangle$. The second-order energy is given by

$$E_K^{(2)}=\langle\psi_K(\gamma_K\mathcal{J}\pi)|V\mathcal{R}V|\psi_K(\gamma_K\mathcal{J}\pi)\rangle. \tag{7}$$

Here $\mathcal{R}$ is the resolvent operator,

$$\mathcal{R}=\mathcal{Q}^{(+)}/(E_K^{(0)}-H_0),$$

$$\mathcal{Q}^{(+)}=\sum_I^{(+)}|\Phi_I^{(+)}(\gamma_I\mathcal{J}\pi)\rangle\langle\Phi_I^{(+)}(\gamma_I\mathcal{J}\pi)|. \tag{8}$$

The projection operator $\mathcal{Q}^{(+)}$ projects onto the subspace spanned by a residual space $\mathfrak{Q}^{(+)}=\mathfrak{D}^{(+)}-\mathfrak{P}^{(+)}$. All the perturbation corrections beyond first order describe relativistic electron correlation [15], including cross contributions between relativistic and correlation effects, i.e., the relativistic many-body shift. When the effective electron-electron interaction is approximated by the instantaneous Coulomb interaction $1/r_{12}$, relativistic electron correlation is termed DC correlation [18]. Inclusion of the frequency-independent Breit interaction in the effective electron-electron interaction yields the no-pair DCB Hamiltonian, and the relativistic electron correlation arising from the DCB Hamiltonian is the DCB correlation [18]. The essential features of the theory are its treatment of the state-specific nondynamical correlation in zero order through an MCDFB SCF and recovery of the remaining correlation, predominantly dynamic pair correlation, by second-order perturbation theory.

Radiative corrections, Lamb shifts, were estimated for each state by evaluating the electron self-energy and vacuum polarization following an approximation scheme discussed by Indelicato, Gorceix, and Desclaux [22]. The code described in Refs. [22] and [23] was adapted to our basis-set expansion calculations for this purpose, and the necessary radial integrals were evaluated analytically. In this scheme [23], the screening of the self-energy is estimated by integrating the charge density of a spinor to a short distance from the origin, typically 0.3 Compton wavelength. The ratio of the integral computed with an MCDFB SCF spinor and that obtained from the corresponding hydrogenic spinor is used to scale the self-energy correction for a bare nuclear charge, which has been computed by Mohr [24].

B. Transition probabilities

The interaction of a single electron with the electromagnetic field is described by the interaction Hamiltonian

$$h_{\mathrm{int}}(\mathbf{r},\omega)=-c\,\boldsymbol{\alpha}\cdot\mathbf{A}(\mathbf{r},\omega)+\phi(\mathbf{r},\omega). \tag{9}$$

Here the four-component potential was expressed as vector potential $\mathbf{A}(\mathbf{r},\omega)$ and scalar potential $\phi(\mathbf{r},\omega)$. It is assumed that the interaction Hamiltonian has incoming photon field time dependence $e^{-i\omega t}$. By multipole expansion of the vector potential $\mathbf{A}(\mathbf{r},\omega)$ and scalar potential $\phi(\mathbf{r},\omega)$ [25], the multipole interaction Hamiltonian $(h_{\mathrm{int}}(\mathbf{r},\omega))_{JM}$ is obtained in

terms of multipole transition operators $t^{\vartheta}_{JM}(\mathbf{r},\omega)$ for the magnetic multipoles ($\vartheta=M$) and electric multipoles ($\vartheta=E$) in the following way:

$$(h_{\rm int}(\mathbf{r},\omega))_{JM}=-ic\sqrt{\frac{(2J+1)(J+1)}{4\pi J}}t^{\vartheta}_{JM}(\mathbf{r},\omega). \quad (10)$$

The matrix elements $\langle t^{M}_{J}\rangle_{ij}$ for magnetic multipole transition between the single-particle states i and j are given as

$$\langle t^{M}_{J}\rangle_{ij}=\langle -\kappa_i||C^{(J)}||\kappa_j\rangle\int\frac{\kappa_i+\kappa_j}{J+1}j_J(kr)\times[P_i(r)Q_j(r)+P_j(r)Q_i(r)]dr. \quad (11)$$

The one-electron reduced matrix elements $\langle t^{E}_{J}\rangle_{ij}$ for transition between the single-particle states i and j are given (see [5,26] for details) in the length form as

$$\langle t^{E(l)}_{J}\rangle_{ij}=\langle\kappa_i||C^{(J)}||\kappa_j\rangle\int\left\{j_J(kr)[P_i(r)P_j(r)+Q_i(r)Q_j(r)]+j_{J+1}(kr)\left(\frac{\kappa_i-\kappa_j}{J+1}[P_i(r)Q_j(r)+P_j(r)Q_i(r)]+[P_i(r)Q_j(r)-P_j(r)Q_i(r)]\right)\right\}dr \quad (12)$$

and in the velocity form as

$$\langle t^{E(v)}_{J}\rangle_{ij}=\langle\kappa_i||C^{(J)}||\kappa_j\rangle\int\left\{\frac{\kappa_j-\kappa_i}{J+1}\left(j'_J(kr)+\frac{j_J(kr)}{kr}\right)\times[P_i(r)Q_j(r)+P_j(r)Q_i(r)]+J\frac{j_J(kr)}{kr}[P_i(r)Q_j(r)-P_j(r)Q_i(r)]\right\}dr, \quad (13)$$

where $j_J(kr)$ is the spherical Bessel function, $\mathbf{k}$ is the photon wave vector, and $k=|\mathbf{k}|$. $C^{(J)}$ is the irreducible tensor of rank J with components related to the spherical harmonics as $C^{(J)}_q=\sqrt{4\pi/(2J+1)}Y^{(J)}_q$. The electromagnetic interaction $H_{\rm int}$ of a many-electron system is the sum of the interactions of all electrons

$$H_{\rm int}=\sum_{ij}\langle h_{\rm int}\rangle_{ij}a^{+}_i a_j \quad (14)$$

as well as the multipole transition operator T^{ϑ}_{JM},

$$T^{\vartheta}_{JM}=\sum_{ij}\langle t^{\vartheta}_{JM}\rangle_{ij}a^{+}_i a_j. \quad (15)$$

The absorption probability $B_{K\to K'}$ per unit time of transition between states $|\psi_K(\gamma_K\mathcal{J}\pi)\rangle$ and $|\psi_{K'}(\gamma_{K'}\mathcal{J}'\pi')\rangle$ with transition energy $\Delta E=h\omega=E_{K'}-E_K$ is equal to the spontaneous-emission probability $A_{K'\to K}$ and is expressed as

$$B^{\vartheta J}{}_{K\to K'}=2\alpha\omega\frac{(2J+1)(J+1)}{(2\mathcal{J}+1)J}[\langle T^{\vartheta}_{J}\rangle_{K'K}]^2=A^{\vartheta J}{}_{K'\to K}. \quad (16)$$

In the lowest order of Rayleigh-Schrödinger perturbation theory, the multipole transition amplitude between states K and K' is

$$\langle T^{\vartheta}_{J}\rangle^{(0)}_{KK'}=\langle\psi_K(\gamma_K\mathcal{J}\pi)|T^{\vartheta}_{JM}|\psi_{K'}(\gamma_{K'}\mathcal{J}'\pi')\rangle=\sum_{II'}C_{IK}C_{I'K'}\langle\Phi^{(+)}_I(\gamma_I\mathcal{J}\pi)|T^{\vartheta}_{JM}|\Phi^{(+)}_{I'}(\gamma_{I'}\mathcal{J}'\pi')\rangle \quad (17)$$

and using the order-by-order expressions of the perturbation series for the state approximated by MCDF SCF wave function $\psi_K(\gamma_K\mathcal{J}\pi)$ of Eq. (3), the next-order transition amplitude is

$$\langle T^{\vartheta}_{J}\rangle^{(1)}_{KK'}=\langle\psi^{(1)}_K(\gamma_K\mathcal{J}\pi)|T^{\vartheta}_{JM}|\psi_{K'}(\gamma_{K'}\mathcal{J}'\pi')\rangle+\langle\psi_K(\gamma_K\mathcal{J}\pi)|T^{\vartheta}_{JM}|\psi^{(1)}_{K'}(\gamma_{K'}\mathcal{J}'\pi')\rangle+\cdots, \quad (18)$$

where the first-order wave function is defined as

$$|\psi^{(1)}_K(\gamma_K\mathcal{J}\pi)\rangle=\mathcal{R}V|\psi_K(\gamma_K\mathcal{J}\pi)\rangle. \quad (19)$$

As with the second-order energy [Eqs. (7) and (8)], the first-order transition amplitude can be expressed in terms of CSFs in the following way:

$$\langle T^{\vartheta}_{J}\rangle^{(1)}_{KK'}=\sum_{L}^{(+)}\sum_{I,I'}^{(+)}C_{IK}C_{I'K'}\times\left(\frac{\langle\Phi^{(+)}_I|V|\Phi^{(+)}_L\rangle\langle\Phi^{(+)}_L|T^{\vartheta}_{JM}|\Phi^{(+)}_{I'}\rangle}{E^{\rm CSF}_I-E^{\rm CSF}_L}+\frac{\langle\Phi^{(+)}_I|T^{\vartheta}_{JM}|\Phi^{(+)}_L\rangle\langle\Phi^{(+)}_L|V|\Phi^{(+)}_{I'}\rangle}{E^{\rm CSF}_{I'}-E^{\rm CSF}_L}\right). \quad (20)$$

One-electron reduced matrix elements $\langle t^{\vartheta}_{J}\rangle_{ij}$ given in Eqs. (11)–(13) are frequency-dependent through spherical Bessel functions $j_J(kr)$. The corrections arising from approximate photon frequency may be eliminated semiempirically using experimental transition energies. In the present study, transition energies (and photon frequencies $\omega^{(0+1+2)}$) calculated by MR-MP second-order perturbation theory are close to the experimental values, and the terms arising from corrections to the photon frequency $\delta\omega=\omega^{\rm expt}-\omega^{(0+1+2)}$ in both zero- and first-order transition amplitudes are significantly smaller and may be neglected. When the first-order corrections to transition probabilities [Eq. (20)] are calculated using second-order MR-MP transition energies, however, the zero-order transition amplitude [Eq. (17)] must also be recalculated using the frequency $\omega^{(0+1+2)}$.

The large and small radial components of the Dirac spinors of symmetry κ are expanded in sets of even-

tempered Gaussian-type functions (GTFs) that satisfy the boundary conditions associated with the finite nucleus [27]. The speed of light is taken to be 137.035 989 5 a.u. throughout this study. The GTFs that satisfy the boundary conditions associated with the finite nucleus are automatically kinetically balanced [27]. For all the systems studied, even-tempered basis sets of $26s22p20d18f15g15h15i15j$ G spinors were employed. The order of the partial-wave expansion ($L_{\max}$), the highest angular momentum of the spinors included in the virtual space, is $L_{\max}=7$ throughout this study. The nuclei were modeled as spheres of uniform proton charge in all calculations. Atomic masses for the Fe^{12+} ($Z=26$), Ni^{14+} ($Z=28$), Zn^{16+} ($Z=30$), Ge^{18+} ($Z=32$), Se^{20+} ($Z=34$), Kr^{22+} ($Z=36$), Sr^{24+} ($Z=38$), Zr^{26+} ($Z=40$), Mo^{28+} ($Z=42$), Rh^{31+} ($Z=45$), Ag^{33+} ($Z=47$), Sn^{36+} ($Z=50$), and Xe^{40+} ($Z=54$) ions are, respectively, 55.847, 58.693, 65.39, 72.61, 78.96, 83.80, 87.62, 91.224, 95.94, 102.9055, 107.8682, 118.710, and 131.29. All electrons have been included in the MR-MP perturbation theory calculations to calculate accurately the effects of relativity on electron correlation.

III. RESULTS AND DISCUSSION

A. Fine-structure term energy separation

MCDFB SCF calculations on the siliconlike ions were performed to obtain a single orthonormal set of spinors for all the lowest $3s^23p^2$ $\mathcal{J}=0$, 1, and 2 fine-structure states by optimizing the $\mathcal{J}$-averaged MC energies [10]:

$$E^{\mathrm{MC}}_{\mathcal{J}\text{-av}}(\gamma_K\mathcal{J}\pi)=\sum_{\mathcal{J}=0,1,2}(2\mathcal{J}+1)E^{\mathrm{MC}}(\gamma_K\mathcal{J}\pi)/\sum_{\mathcal{J}'}(2\mathcal{J}'+1) \tag{21}$$

instead of performing state-specific MCDFB calculations on each fine-structure state. The approach is especially effective for computing small fine-structure splittings (i.e., near-degeneracy among the $3p_{1/2}$ and $3p_{3/2}$ spinors). The MCDFB SCF is a complete active space SCF [9,10] within the $n=3$ $(3s_{1/2},3p_{1/2},3p_{3/2},3d_{3/2},3d_{5/2})$ spinor subspace. In the MCDFB SCF calculations, the $1s_{1/2}$, $2s_{1/2}$, and $2p_{1/2,3/2}$ spinors were kept fully occupied, and the remaining four electrons were treated as active electrons in generating complete active space CSFs within the subspace. Thus, the numbers of CSFs generated are, respectively, 29, 45, and 70, for the $\mathcal{J}=0$, 1, and 2 states. Following the MCDFB SCF calculations, state-specific MR-MP calculations were carried out on each of the lowest $^3P_{\mathcal{J}}$ ($\mathcal{J}=0,1,2$) fine-structure states of the siliconlike ions employing the orthonormal set of spinors. Table I displays the computed MCDFB SCF energies (E_{MCDFB}), Lamb shifts (LS), second-order DC correlation corrections ($E^{(2)}_{\mathrm{DC}}$), and second-order Breit interaction energies ($B^{(2)}$) of the $^3P_{0,1,2}$ even-parity states of Fe^{12+} ($Z=26$) through Xe^{40+} ($Z=54$).

Among the numerous CSFs included in the MCDFB SCF, the electronic configurations $3s^23p^2_{1/2}$ and $3s^23p^2_{3/2}$ especially interact strongly in low- and intermediate-Z species. The $3p_{1/2}$ and $3p_{3/2}$ spinors are nearly degenerate in the Fe^{12+} ($Z=26$) ion because relativistic effects, e.g., the spin-orbit interaction, are not large, and thus the CSFs arising from $3s^23p^2_{1/2}$ and $3s^23p^2_{3/2}$ configurations are nearly degenerate, and there is a strong configuration interaction between them. For the lowest $\mathcal{J}=0$ ($^3P_0$) state of Fe^{12+}, the MCDF SCF calculations yield configuration mixing coefficients nearly equal in magnitude, 0.8924 and -0.4126, respectively, for the two CSFs arising from the $3s^23p^2_{1/2}$ and

TABLE I. First-order energies (E_{MCDFB}), Lamb shifts (LS), second-order Dirac-Coulomb correlation energies ($E^{(2)}_{\mathrm{DC}}$), and second-order Breit correlation corrections ($B^{(2)}$) of the fine-structure components $3s^23p^2\,{}^3P_{\mathcal{J}}$. Energies are in atomic units.

Z	E_{MCDFB}	LS	$E^{(2)}_{\mathrm{DC}}$	$B^{(2)}$
$3s^23p^2\,{}^3P_0$				
26	−1210.265253	0.312364	−0.498968	−0.019258
28	−1427.998246	0.402883	−0.503985	−0.022850
30	−1664.395044	0.510152	−0.508534	−0.026715
32	−1919.603328	0.635785	−0.512917	−0.030959
34	−2193.784675	0.781448	−0.517071	−0.035564
36	−2487.115354	0.948860	−0.521049	−0.040452
38	−2799.786683	1.139796	−0.524879	−0.045884
40	−3132.005530	1.356095	−0.528591	−0.051613
42	−3483.995009	1.599657	−0.532201	−0.057653
45	−4049.581628	2.020504	−0.537468	−0.067780
47	−4452.092554	2.341131	−0.540909	−0.075030
50	−5094.758460	2.887733	−0.546027	−0.086783
54	−6025.951504	3.751621	−0.552828	−0.104222
$3s^23p^2\,{}^3P_1$				
26	−1210.220553	0.312460	−0.501478	−0.019268
28	−1427.927750	0.403037	−0.506685	−0.022814
30	−1664.287843	0.510387	−0.511482	−0.026501
32	−1919.445556	0.636129	−0.515915	−0.030682
34	−2193.559300	0.781932	−0.520031	−0.035211
36	−2486.801951	0.949516	−0.523884	−0.040087
38	−2799.361237	1.140661	−0.527528	−0.045355
40	−3131.440209	1.357205	−0.531003	−0.050978
42	−3483.257890	1.601054	−0.534348	−0.056856
45	−4048.517324	2.022412	−0.539192	−0.066814
47	−4450.756767	2.343436	−0.542343	−0.073911
50	−5092.922223	2.890724	−0.547006	−0.085394
54	−6023.242682	3.755697	−0.553209	−0.102369
$3s^23p^2\,{}^3P_2$				
26	−1210.174789	0.312511	−0.505359	−0.019288
28	−1427.867054	0.403096	−0.510883	−0.022834
30	−1664.211146	0.510450	−0.516112	−0.026499
32	−1919.352554	0.636191	−0.521032	−0.030690
34	−2193.450242	0.781990	−0.525653	−0.035203
36	−2486.677368	0.949568	−0.529984	−0.040078
38	−2799.221748	1.140707	−0.534050	−0.045344
40	−3131.286406	1.357246	−0.537881	−0.051024
42	−3483.090302	1.601089	−0.541520	−0.056892
45	−4048.329901	2.022439	−0.546695	−0.066873
47	−4450.556589	2.343458	−0.550010	−0.073997
50	−5092.703488	2.890738	−0.554854	−0.085474
54	−6023.000106	3.755698	−0.561193	−0.102445

TABLE II. Leading configuration-mixing coefficients of the $3s^2 3p^{2\,3}P_{0,1,2}$ states of ions along the silicon isoelectronic sequence.

Z	J	$C_{3s^2 3p_{1/2}^2}$	$C_{3s^2 3p_{1/2} 3p_{3/2}}$	$C_{3s^2 3p_{3/2}^2}$
26	0	0.8924		−0.4126
	1		0.9833	
	2		0.7674	0.6139
36	0	0.9617		−0.2260
	1		0.9877	
	2		0.9500	0.2695
42	0	0.9787		−0.1506
	1		0.9898	
	2		0.9770	0.1572
54	0	0.9917		−0.0705
	1		0.9934	
	2		0.9910	0.0639

$3s^2 3p_{3/2}^2$ (Table II). As Z increases, relativity lifts the near-degeneracy and significantly weakens the configuration interaction between the two CSFs because it induces a large separation between the $3p_{1/2}$ and $3p_{3/2}$ spinor energies and simultaneously a smaller separation between the $3s_{1/2}$ and $3p_{1/2}$ spinor energies [28]. Table II displays just such a trend as the nuclear charge increases. The MCDF SCF on the $\mathcal{J}=0$ state of Xe^{40+} ($Z=54$) yields configuration mixing coefficients of 0.9917 and −0.0705, respectively, for the two CSFs arising from $3s^2 3p_{1/2}^2$ and $3s^2 3p_{3/2}^2$. Configuration interaction between the two CSFs for Xe^{40+} is reduced dramatically by relativity, making $3s^2 3p_{1/2}^2$ the dominant configuration. A complete active space SCF [10] within the $n=3$ complex gives rise to 45 CSFs for the $\mathcal{J}=1$, even-parity state, the electronic configuration $3s^2 3p_{1/2} 3p_{3/2}$ being the dominant confguration with mixing coefficients of 0.9833 for $Z=26$ and 0.9934 for $Z=54$. Thus the $\mathcal{J}=1$ state does not exhibit near-degeneracy in the low- to high-Z series. The $\mathcal{J}=2$, even-parity CSFs behave like those of the $\mathcal{J}=0$ state,

TABLE III. Energy levels (cm^{-1}) of the $3s^2 3p^{2\,3}P_{1,2}$ fine-structure components relative to the ground $3s^2 3p^{2\,3}P_0$ state. Values in parentheses are the deviations from experiment of the calculated fine-structure intervals.

Z	E_{MCDFB}	$E_{\mathrm{MR\text{-}MP}}$	Huang [a] [4]	Kohstall *et al.* [b] [30]	Expt. [c]
$3s^2 3p^{2\,3}P_1$					
26	9831(−528)	9278(25)	9219(84)	9185(118)	9302.5
28	15506(−588)	14922(−4)	14758(160)		14917.5
30	23579(−623)	22979(−23)	22709(247)	22711(245)	22956
32	34702(−625)	34105(−38)	33725(352)		34076.7
34	49570(−614)	48998(−42)	48507(449)		48956
36	68928(−559)	68386(−17)	67801(568)	67813(556)	68369
38	93564(−474)	93099(−9)	92395(695)		93090
40	124317(−395)	123927(−7)	123122(798)		123920
42	162086(−356)	161790(−60)	160875(855)		161730
45	234007	233841	232789		
47	293677	293610	292456		
50	403664	403754	402435		
54	595412	595735	594139		
$3s^2 3p^{2\,3}P_2$					
26	19887(−1326)	18478(83)	18694(−133)	18453(108)	18561.0
28	28840(−1463)	27330(47)	27607(−230)		27376.5
30	40426(−1585)	38810(31)	39191(−350)	38677(164)	38841
32	55128(−1715)	53406(7)	53905(−495)		53412.5
34	73518(−1823)	71714(−19)	72315(−620)		71695
36	96282(−1885)	94403(−6)	95098(−701)	94093(304)	94397
38	124189(−1848)	122295(46)	123024(−683)		122341
40	158082(−1854)	156173(55)	156936(−708)		156228
42	198875(−1866)	196997(12)	197746(−737)		197009
45	275147	273321	274045		
47	337616	335845	336524		
50	451674	450024	450587		
54	648652	647206	647520		

[a]Huang [4], $n=3$ complex finite-difference MCDF calculations.
[b]$n=3,4,5$ MCDF calculations by Kohstall *et al.* from Ref. [30].
[c]NIST experimental data from Ref. [29].

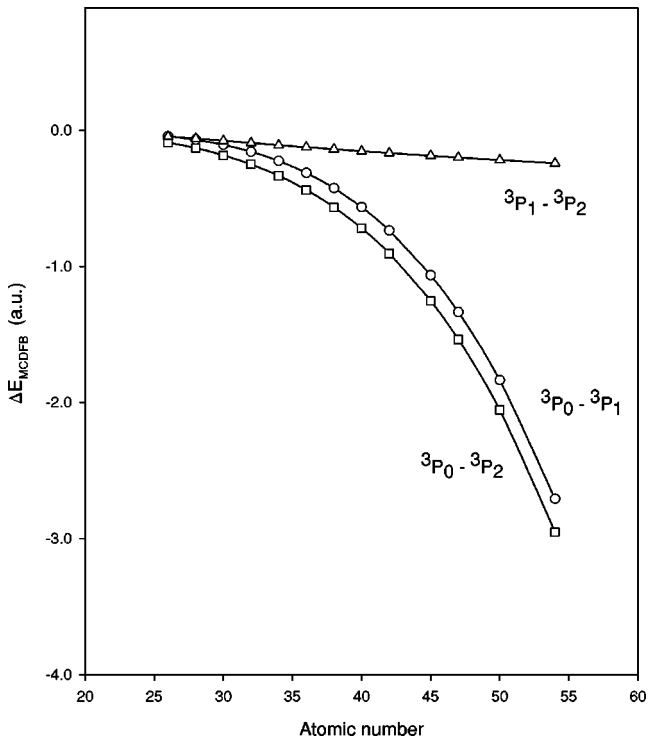

FIG. 1. Contributions of the first-order MCDFB energies to the $3s^2 3p^2$ fine-structure intervals.

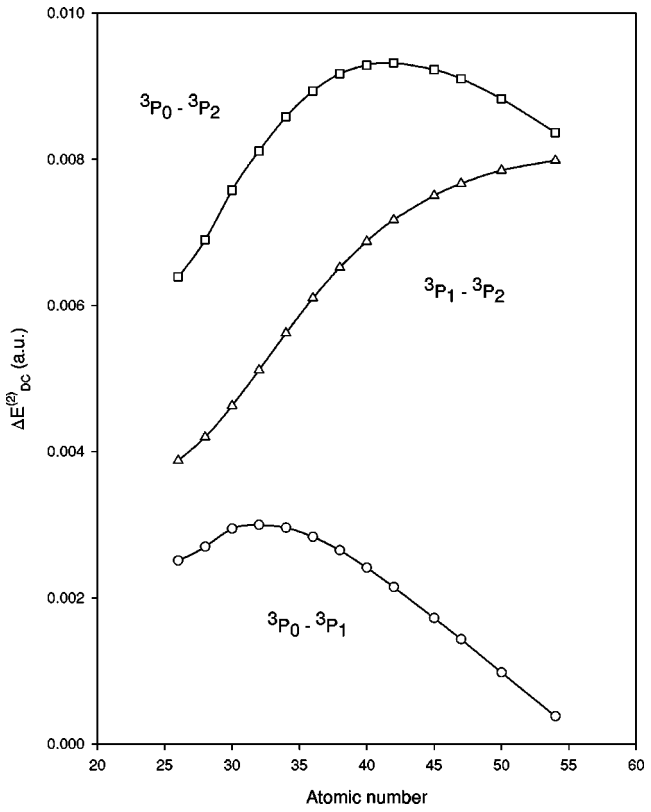

FIG. 2. Contributions of the second-order Dirac-Coulomb correlation energies to the $3s^2 3p^2$ fine-structure intervals.

dispaying near-degeneracy and strong configuration interaction.

In Table III, a detailed comparison of theoretical and experimental data is made on the fine-structure term energies (cm^{-1}) relative to the ground $\mathcal{J}=0$ ($3s^2 3p^2\ ^3P_0$) state. Experimental fine-structure intervals [29] are reproduced in the last column for comparison. Theoretical MCDFB and MR-MP term energy separations of the $^3P_1$ ($\mathcal{J}=1$) and $^3P_2$ ($\mathcal{J}=2$), given, respectively, in the second and third columns of the table, were computed by subtracting the total MCDFB and MR-MP energies of the ground $\mathcal{J}=0$ ($3s^2 3p^2\ ^3P_0$) state from those of the $\mathcal{J}=1$ and $\mathcal{J}=2$ levels. The fourth and fifth columns contain the fine-structure intervals obtained, respectively, by Huang [4] and Kohstall *et al.* [30] in large-scale MCDF SCF calculations for comparison.

Most of the experimentally determined fine-structure intervals are reproduced by the complete active space MCDFB calculations within the $n=3$ complex, which account for nondynamical correlation (quasidegeneracy). In Fe^{12+}, the lowest $^3P_1$ ($\mathcal{J}=1$) and $^3P_2$ ($\mathcal{J}=2$) state energies computed are, respectively, 9831 cm^{-1} and 19 887 cm^{-1} above the ground $^3P_0$ ($\mathcal{J}=0$) state, while experimental values are, respectively, 9303 cm^{-1} and 18 561 cm^{-1} [29]. For Mo^{28+} ($Z=42$), the lowest $^3P_1$ ($\mathcal{J}=0$) and $^3P_2$ ($\mathcal{J}=1$) state energies computed in MCDFB SCF calculations are, respectively, 162 086 cm^{-1} and 198 875 cm^{-1} above the ground $^3P_0$ ($\mathcal{J}=2$) state, while the corresponding experimental values are, respectively, 161 730 cm^{-1} and 197 009 cm^{-1}. The residual discrepancy is primarily due to dynamic correlation and radiative corrections unaccounted for in the MCDFB SCF calculations. Our MR-MP perturbation theory accurately accounts for both nondynamical and dynamical correlation [9,15]. The term energy separations in column 3, computed with MR-MP and corrected by the Lamb shifts, dramatically improve over those computed with MCDFB SCF, in excellent agreement with experiment throughout the isoelectronic sequence. Values in parentheses are the deviations from experiment of the calculated fine-structure intervals. The deviations between the computed and experimental $^3P_1$-$^3P_0$ fine-structure intervals range from a mere 4 cm^{-1} at $Z=28$ to 60 cm^{-1} at $Z=42$. The small, but uneven, deviations from experiment of the calculated fine-structure intervals with no clear Z-dependent trend are most likely due to the J-averaged MCDFB SCF employed to generate zero-order wave functions. The deviations from experiment of the J-averaged MCDFB SCF energies fail to show any clear Z-dependent trend, while in the state-specific MCDF SCF calculations of Huang and Kohstall *et al.*, the deviations increase monotonically as Z increases.

Figures 1–4 show the contributions from each order of perturbation theory to the $3s^2 3p^2$ fine-structure intervals. The contributions of the first-order (MCDFB) energies ($\Delta E_{\mathrm{MCDFB}}$), second-order Dirac-Coulomb correlation energies ($\Delta E^{(2)}_{\mathrm{DC}}$), second-order Breit interaction energies ($\Delta B^{(2)}$), and the Lamb shifts (Δ LS) to the $3s^2 3p^2$ fine-structure intervals are displayed, respectively, in Figs. 1, 2, 3, and 4 as functions of atomic number Z. The MCDFB SCF and MR-MP calculations, as well as the Lamb shifts, result in significant corrections and yield close agreement between

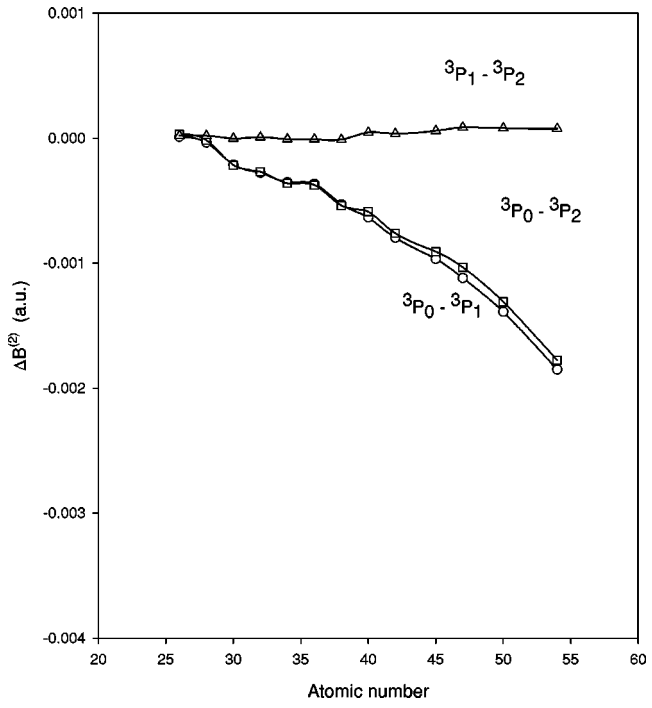

FIG. 3. Contributions of the second-order Breit interaction energies to the $3s^2 3p^2$ fine-structure intervals.

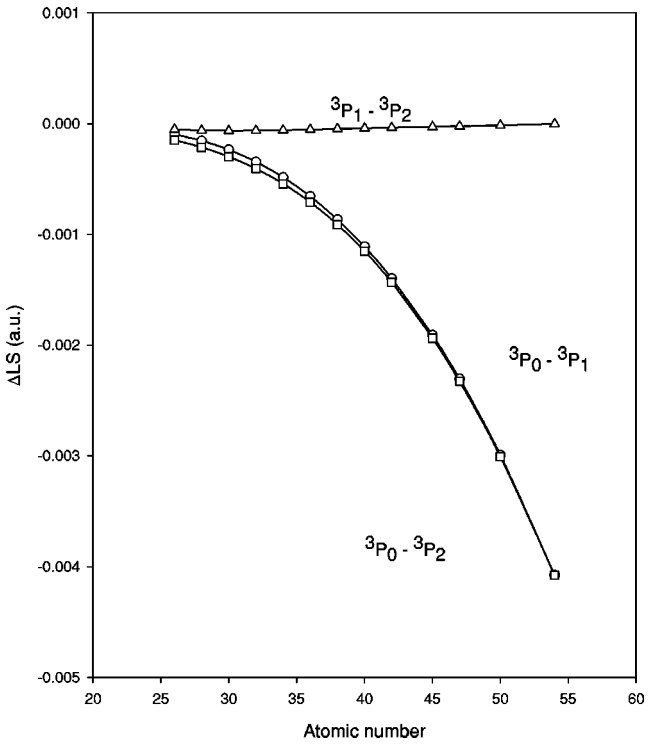

FIG. 4. Contributions of the Lamb shifts to the $3s^2 3p^2$ fine-structure intervals.

the calculated and experimental fine-structure intervals. The largest contribution to the fine-structure term energy separations comes from the first-order MCDFB energies by which the bulk of the separations are reproduced. However, the figures exemplify the importance of $\Delta E_{\mathrm{DC}}^{(2)}$ and Δ LS in accurately predicting fine-structure term energy separations. The Lamb shift correction Δ LS is small at the low-Z end, but increases rapidly as Z increases and becomes comparable in magnitude at the large-Z end with the second-order Dirac-Coulomb correlation energies, $\Delta E_{\mathrm{DC}}^{(2)}$.

B. Magnetic-dipole and electric-quadrupole transition probabilities among the $3s^2 3p^2\ ^3P_{\mathcal{J}}$ fine-structure states

The theoretical $M1$ and $E2$ transition probabilities among the $3s^2 3p^2\ ^3P_{\mathcal{J}}$ ($\mathcal{J}=0,1,2$) fine-structure states of the $Z=26$–54 siliconlike ions were computed using the MCDFB SCF and MR-MP wave functions. To evaluate them, we followed the method outlined in Sec. II. In Table IV, we list the $M1$ and $E2$ transition probabilities for the $3s^2 3p^2\ ^3P_2$-$^3P_1$ transition. In each entry, $E2$ transition probabilities computed in both the length (l) and velocity (v) forms are given to see the level of agreement between the two forms for electric-quadrupole transition probabilities. Available experimental fine-structure intervals are given in the third column for $Z=26$ through 42. In columns 4 and 5, theoretical fine-structure intervals and $M1$ and $E2$ transition probabilities computed with MCDFB SCF wave functions are given. In columns 6 and 7, we list those computed with MR-MP wave functions. In the last two columns, Huang's theoretical results [4] are given for comparison. The values from Ref. [4] were obtained using state-specific MCDF SCF. The spinors of different $\mathcal{J}$ states optimized in state-specific MCDF SCF are nonorthogonal, which explains the noticeable differences between our MCDFB results and Huang's for low-Z ions. As Z increases, the fine-structure intervals and $M1$ and $E2$ transition probabilities computed with our $\mathcal{J}$-averaged MCDFB SCF agree with those computed with state-specific MCDF SCF. The $M1$ transition probabilities computed with MR-MP wave functions, which account for dynamical correlation, are consistently smaller in magnitude than those computed with MCDFB wave functions. Theoretical $M1$ transition probabilities computed with MR-MP wave functions increase by two orders of magnitude as Z increases, from 9.586 s^{-1} at $Z=26$ to 7.310×10^2 s^{-1} at $Z=54$. $E2$ transition probabilities are consistently four orders of magnitude smaller than the corresponding $M1$ transition probabilities throughout the range of Zs. Thus the $^3P_2$-$^3P_1$ transition is dominated by the magnetic-dipole decay. There is a significant disagreement between the length and velocity forms of the computed $E2$ transition probabilities at the low-Z end because of its minute magnitude and because the contributions from negative-energy states are not accounted for to ensure gauge independence [5,6]. The agreement between the two forms improves, to within about 10% for $Z\geqslant30$, with increasing Z along the isoelectronic sequence. The disagreement between the length and velocity forms computed with MCDFB SCF wave functions, however, remains large along the isoelectronic sequence.

In Table V, we list the $M1$ transition probabilities, A_{MCDFB}^{M1} and $A_{\mathrm{MR\text{-}MP}}^{M1}$, for the $3s^2 3p^2\ ^3P_1$-$^3P_0$ transition computed, respectively, with MCDFB and MR-MP wave functions. Available experimental fine-structure intervals are given in the second column for $Z=26$ through 42. In col-

TABLE IV. Theoretical $M1$ and $E2$ transition probabilities (s^{-1}) between the fine-structure components $3s^2 3p^2$ ($^3P_2$-$^3P_1$) along the silicon isoelectronic sequence.

			This work				Previous work [4]	
Z	Type	ΔE_{expt}	ΔE_{MCDFB}	A_{MCDFB}	$\Delta E_{\text{MR-MP}}$	$A_{\text{MR-MP}}$	ΔE^{MCDF} [a]	A_{MCDF} [a]
26	$M1$	9259	10056	1.249(+1)	9200	9.586(+0)	9475	1.057(+1)
	$E2(l)$			5.840(−4)		3.557(−4)		4.093(−4)
	$E2(v)$			4.382(−3)		6.038(−4)		
28	$M1$	12459	13334	2.745(+1)	12408	2.216(+1)	12849	2.485(+1)
	$E2(l)$			1.460(−3)		9.694(−4)		1.150(−3)
	$E2(v)$			8.266(−3)		1.439(−3)		
30	$M1$	15895	16847	5.123(+1)	15831	4.254(+1)	16482	4.850(+1)
	$E2(l)$			2.944(−3)		2.027(−3)		2.509(−3)
	$E2(v)$			1.308(−2)		2.168(−3)		
32	$M1$	19336	20426	8.351(+1)	19301	7.053(+1)	20180	8.124(+1)
	$E2(l)$			4.948(−3)		3.519(−3)		4.435(−3)
	$E2(v)$			1.779(−2)		3.821(−3)		
34	$M1$	22739	23948	1.227(+2)	22716	1.047(+2)	23808	1.213(+2)
	$E2(l)$			7.223(−3)		5.246(−3)		6.680(−3)
	$E2(v)$			2.167(−2)		5.756(−3)		
36	$M1$	26028	27354	1.673(+2)	26017	1.439(+2)	27297	1.668(+2)
	$E2(l)$			9.521(−3)		7.074(−3)		8.975(−3)
	$E2(v)$			2.444(−2)		8.363(−3)		
38	$M1$	29251	30625	2.166(+2)	29196	1.877(+2)	30629	2.171(+2)
	$E2(l)$			1.169(−2)		8.756(−3)		1.115(−2)
	$E2(v)$			2.631(−2)		9.743(−3)		
40	$M1$	32308	33765	2.706(+2)	32246	2.359(+2)	33814	2.718(+2)
	$E2(l)$			1.368(−2)		1.038(−2)		1.315(−2)
	$E2(v)$			2.749(−2)		1.152(−2)		
42	$M1$	35279	36789	3.294(+2)	35207	2.873(+2)	36871	3.314(+2)
	$E2(l)$			1.549(−2)		1.179(−2)		1.496(−2)
	$E2(v)$			2.824(−2)		1.313(−2)		
45	$M1$		41140	4.278(+2)	39480	3.784(+2)	41256	4.308(+2)
	$E2(l)$			1.788(−2)		1.398(−2)		1.736(−2)
	$E2(v)$			2.888(−2)		1.548(−2)		
47	$M1$		43939	5.008(+2)	42235	4.454(+2)	44068	5.044(+2)
	$E2(l)$			1.930(−2)		1.526(−2)		1.878(−2)
	$E2(v)$			2.915(−2)		1.687(−2)		
50	$M1$		48010	6.223(+2)	46270	5.576(+2)	48152	6.267(+2)
	$E2(l)$			2.121(−2)		1.704(−2)		2.070(−2)
	$E2(v)$			2.951(−2)		1.877(−2)		
54	$M1$		53240	8.084(+2)	51471	7.310(+2)	55381	8.133(+2)
	$E2(l)$			2.343(−2)		1.918(−2)		2.289(−2)
	$E2(v)$			2.989(−2)		2.104(−2)		

[a]Huang [4], $n=3$ complex finite-difference MCDF calculations.

umns 3 and 4, respectively, theoretical fine-structure intervals and A^{M1}_{MCDFB} are presented. In columns 5 and 6, we list those computed with MR-MP wave functions. Theoretical $M1$ transition probabilities $A^{M1}_{\text{MR-MP}}$ increase by five orders of magnitude as Z increases, from 1.385×10^{1} s^{-1} at $Z=26$ to 2.743×10^{6} s^{-1} at $Z=54$. In the last two columns, Huang's theoretical results [4], computed using state-specific MCDF SCF, are given for comparison. The transition probabilities computed with MR-MP wave functions are seen to be consistently smaller than those computed with MCDFB SCF wave functions, indicating the importance of dynamical correlation in computing the fine-structure interval and wave functions. Towards the large-Z end, however, the fine-structure intervals and transition probabilities, A^{M1}_{MCDFB} and $A^{M1}_{\text{MR-MP}}$, computed with the two wave functions agree well, indicating that the dynamical correlation has small contributions for large-Z ions.

In Table VI, we list the $E2$ transition probabilities, A^{E2}_{MCDFB} and $A^{E2}_{\text{MR-MP}}$, for the $^3P_2$-$^3P_0$ of siliconlike ions computed, respectively, with MCDFB SCF and MR-MP

TABLE V. Theoretical $M1$ transition probabilities (s^{-1}) between the fine-structure components $3s^2 3p^2$ ($^3P_1$-$^3P_0$) in siliconlike ions.

		This work				Previous work [4]	
Z	ΔE_{expt}	ΔE_{MCDFB}	A^{M1}_{MCDFB}	$\Delta E_{\text{MR-MP}}$	$A^{M1}_{\text{MR-MP}}$	$\Delta E^{\text{MCDF a}}$	A^{M1}_{MCDF} [a]
26	9303	9831	1.643(+1)	9278	1.385(+1)	9219	1.358(+1)
28	14918	15506	6.329(+1)	14922	5.642(+1)	14758	5.466(+1)
30	22956	23579	2.177(+2)	22979	2.007(+2)	22709	1.947(+2)
32	34077	34702	6.771(+2)	34105	6.404(+2)	33725	6.214(+2)
34	48956	49570	1.944(+3)	48998	1.851(+3)	48507	1.799(+3)
36	68369	68928	5.033(+3)	68386	4.906(+3)	67801	4.781(+3)
38	93090	93564	1.227(+4)	93099	1.206(+4)	92395	1.178(+4)
40	123920	124317	2.800(+4)	123927	2.777(+4)	123122	2.719(+4)
42	161730	162086	6.086(+4)	161790	6.050(+4)	160875	5.927(+4)
45		234007	1.777(+5)	233841	1.771(+5)	232789	1.742(+5)
47		293677	3.452(+5)	293610	3.446(+5)	292456	3.392(+5)
50		403664	8.759(+5)	403754	8.758(+5)	402435	8.635(+5)
54		595412	2.740(+6)	595735	2.743(+6)	594139	2.708(+6)

[a]Huang [4], $n=3$ complex finite-difference MCDF calculations.

TABLE VI. Theoretical $E2$ transition probabilities (s^{-1}) between the fine-structure components $3s^2 3p^2$ ($^3P_2$-$^3P_0$) along the silicon isoelectronic sequence.

			This work				Previous work [4]	
Z	Type	ΔE_{expt}	ΔE_{MCDFB}	A^{E2}_{MCDFB}	$\Delta E_{\text{MR-MP}}$	$A^{E2}_{\text{MR-MP}}$	$\Delta E^{\text{MCDF a}}$	A^{E2}_{MCDF} [a]
26	(l)	18561	19887	4.068(−3)	18478	2.618(−3)	18694	6.535(−3)
	(v)			1.167(−1)		1.211(−2)		
28	(l)	27377	28840	2.187(−2)	27330	1.571(−2)	27607	3.135(−2)
	(v)			4.081(−1)		5.008(−2)		
30	(l)	38841	40426	1.004(−1)	38810	7.604(−2)	39191	1.298(−1)
	(v)			1.290(+0)		1.169(−1)		
32	(l)	53413	55128	3.999(−1)	53406	3.203(−1)	53905	4.757(−1)
	(v)			3.709(+0)		4.318(−1)		
34	(l)	71691	73518	1.412(+0)	71714	1.178(+0)	72315	1.581(+0)
	(v)			9.881(+0)		1.445(+0)		
36	(l)	94397	96282	4.612(+0)	94403	3.920(+0)	95098	4.847(+0)
	(v)			2.472(+1)		4.634(+0)		
38	(l)	122341	124189	1.330(+1)	122295	1.174(+1)	123024	1.390(+1)
	(v)			5.901(+1)		1.292(+1)		
40	(l)	156228	158082	3.660(+1)	156173	3.300(+1)	156936	3.759(+1)
	(v)			1.352(+2)		3.519(+1)		
42	(l)	197009	198875	9.503(+1)	196997	8.701(+1)	197746	9.655(+1)
	(v)			2.996(+2)		9.099(+1)		
45	(l)		275147	3.621(+2)	273321	3.376(+2)	274045	3.644(+2)
	(v)			9.777(+2)		3.460(+2)		
47	(l)		337616	8.366(+2)	335845	7.871(+2)	336524	8.390(+2)
	(v)			1.930(+3)		8.003(+2)		
50	(l)		451674	2.735(+3)	450024	2.602(+3)	450587	2.736(+3)
	(v)			5.492(+3)		2.624(+3)		
54	(l)		648652	1.184(+4)	647206	1.138(+4)	647520	1.182(+4)
	(v)			2.054(+4)		1.140(+4)		

[a]Huang [4], $n=3$ complex finite-difference MCDF calculations.

TABLE VII. Theoretical lifetimes (s) of the $3s^2 3p^2\,{}^3P_2$ and ${}^3P_1$ fine-structure states of ions along the silicon isoelectronic sequence.

	$3s^2 3p^2\,{}^3P_1$		$3s^2 3p^2\,{}^3P_2$	
Z	τ_{MCDFB}	$\tau_{\text{MR-MP}}$	τ_{MCDFB}	$\tau_{\text{MR-MP}}$
26	6.086(−2)	7.220(−2)	8.003(−2)	1.043(−1)
28	1.580(−2)	1.772(−2)	3.640(−2)	4.509(−2)
30	4.593(−3)	4.713(−3)	1.948(−2)	2.072(−2)
32	1.477(−3)	1.503(−3)	1.192(−2)	1.260(−2)
34	5.144(−4)	5.263(−4)	8.057(−3)	9.444(−3)
36	1.987(−4)	2.038(−4)	5.817(−3)	6.765(−3)
38	8.150(−5)	8.292(−5)	4.349(−3)	5.014(−3)
40	3.571(−5)	3.601(−5)	3.255(−3)	3.719(−3)
42	1.643(−5)	1.653(−5)	2.356(−3)	2.671(−3)
45	5.627(−6)	5.646(−6)	1.266(−3)	1.397(−3)
47	2.897(−6)	2.902(−6)	7.477(−4)	8.113(−4)
50	1.142(−6)	1.142(−6)	2.979(−4)	3.165(−4)
54	3.650(−7)	3.646(−7)	7.906(−5)	8.257(−5)

wavefunctions in both the length and velocity forms. In columns 4 and 5, respectively, theoretical fine-structure intervals and A^{M1}_{MCDFB} are given. In columns 6 and 7, we list those computed with MR-MP wave functions. In the last two columns, Huang's theoretical results [4] are given for comparison. Like in the ${}^3P_2$-${}^3P_1$ transition, there is a significant disagreement between the length and velocity forms of the computed $E2$ transition probabilities at the low-Z end because contributions from negative energies are not included to ensure agreement between the two forms [5,6]. The agreement between the two forms computed with MR-MP wave functions improves to within 10% with increasing Z ($\geqslant 38$) along the isoelectronic sequence. Again the disagreement between the length and velocity forms computed with MCDFB SCF wave functions remains large along the isoelectronic sequence.

Table VII gives the MCDFB and MR-MP theoretical lifetimes, τ_{MCDFB} and $\tau_{\text{MR-MP}}$, respectively, of the $3s^2 3p^2\,{}^3P_{1,2}$ states of ions along the silicon isoelectronic sequence. They were computed by summing the $M1$ and $E2$ transition probabilities given in Tables IV, V, and VI to all possible lower levels. The length form of the $E2$ transition probabilities was employed to evaluate the theoretical lifetimes throughout Z

TABLE VIII. Comparison of the theoretical and experimental lifetimes (ms) of the $3s^2 3p^2\,{}^3P_2$ state Kr^{22+} ($Z=36$) ion.

	τ^{M1}		$\tau^{M1+E2(l)}$		$\tau^{M1+E2(v)}$	
τ_{expt}	MCDFB	MR-MP	MCDFB	MR-MP	MCDFB	MR-MP
	5.977	6.949	5.817	6.765	5.207	6.732
5.7±0.5 [a]						
6.3±0.3 [b]						
6.8±0.1 [c]						

[a]Experiment, Ref. [13].
[b]Experiment, Ref. [14].
[c]Experiment, Ref. [12].

TABLE IX. Percentage contribution of the multipole transition probabilities (s^{-1}) contributing to the lifetime of $3s^2 3p^2\,{}^3P_2$ state of ions along the silicon isoelectronic sequence.

	$E2\ 3s^2 3p^2\ ({}^3P_2$-${}^3P_0)$		$M1\ 3s^2 3p^2\ ({}^3P_2$-${}^3P_1)$	
Ion	$A^{E2}_{\text{MR-MP}}$	percentage	$A^{M1}_{\text{MR-MP}}$	percentage
Fe^{12+} ($Z=26$)	2.6(−3)	0.03	9.6(+0)	99.97
Kr^{22+} ($Z=36$)	3.9(+0)	3	1.4(+2)	97
Mo^{28+} ($Z=42$)	8.7(+1)	23	2.9(+2)	77
Xe^{40+} ($Z=54$)	1.1(+4)	94	7.3(+2)	6

because it is less sensitive to negative energy contributions [5,6]. For the $3s^2 3p^2\,{}^3P_1$ fine-structure level of siliconlike ions, lifetimes decrease by five orders of magnitude as Z increases, ranging from 7.22×10^{-2} s at $Z=26$ to 3.65×10^{-7} s at $Z=54$, while for the $3s^2 3p^2\,{}^3P_2$ state, there is a decrease of four orders of magnitude.

Table VIII compares the theoretical lifetimes of the $3s^2 3p^2\,{}^3P_2$ state of Kr^{22+} ($Z=36$) with those obtained in recent experiments [12–14]. Experimental lifetimes τ_{expt} measured in three recent experiments [12–14] are listed in the first column. The theoretical lifetimes τ^{M1} of the ${}^3P_2$ state evaluated solely using the $M1$ transition probabilities (ignoring the contribution of the $E2$ transition probabilities) are given in the next two columns, each evaluated, respectively, with the MCDFB SCF and MR-MP wave functions. The lifetimes $\tau^{M1+E2(l)}$ evaluated using $M1$ and the length form of the $E2$ transition probabilities are given, respectively, in the fourth and fifth columns for MCDFB and MR-MP wave functions. In the last two columns, we list the lifetimes $\tau^{M1+E2(v)}$ evaluated with $M1$ and the velocity form of the $E2$ transition probabilities. The lifetimes computed with MCDFB SCF wave functions are consistently lower than those computed with MR-MP wave functions, and apparently support the smallest experimental lifetime of 5.7 ± 0.5 ms [13]. We believe this is primarily because the theoretical fine-structure intervals computed with MCDFB SCF wave functions are insufficiently accurate since the method fails to account for a significant fraction of dynamical correlation. However, the lifetimes computed with the correlated MR-MP wave functions are in the range 6.73–6.95 ms, clearly supporting the latest experimental lifetime of 6.8 ± 0.1 ms [12]. Our MR-MP theoretical lifetimes computed in the length and velocity forms agree with this lifetime to within the experimental error limit. The radiative decay of the ${}^3P_2$ state Kr^{22+} occurs predominantly via the magnetic-dipole ${}^3P_2$-${}^3P_1$ transition.

Table IX displays percentage contributions of the $E2(l)$ and $M1$ transition probabilities to the lifetimes of the ${}^3P_2$ state of siliconlike ions. Percentage contributions of the $E2$ and $M1$ transition probabilities to the lifetime of the ${}^3P_2$ state Fe^{12+} ($Z=26$) ion are, respectively, 0.03% and 99.97%, while they are, respectively, 94% and 6% for Xe^{40+}. Thus for low-Z ions, the radiative decay of the ${}^3P_2$ state is predominantly via the magnetic-dipole ${}^3P_2$-${}^3P_1$ transition, while it occurs via the electric-quadrupole ${}^3P_2$-${}^3P_0$ transition for high-Z ions.

IV. CONCLUSION

Relativistic MR-MP perturbation theory has been employed to calculate the transition energies and magnetic-dipole and electric-quadrupole transition probabilities of siliconlike ions. As a zero-order approximation, a large $n=3$ complex reference space was chosen. The calculated second-order MR-MP transition energies for various siliconlike ions ($26 \leqslant Z \leqslant 54$) are the most accurate among those obtained with various relativistic methods. Such accuracy may be achieved only with a fully relativistic many-body theory that accounts for one-body kinematic relativistic effects, relativistic nondynamic and dynamic correlation corrections, and the Lamb shifts. The correlation corrections due to the Coulomb and Breit interactions to the $E2$ and $M1$ transition operator have been accounted for in the first-order MR-MP wave functions. The contributions of the $M1$ and $E2$ transition probabilities to the lifetimes of the $3s^2 3p^2\,{}^3P_{1,2}$ have been analyzed.

ACKNOWLEDGMENTS

The authors thank E. Träbert of Ruhr-Universität Bochum for providing us with unpublished data. This work has been supported by the US-Israel Binational Science Foundation.

[1] E. Träbert, P. H. Heckmann, R. Hutton, and I. Martinson, J. Opt. Soc. Am. B **5**, 2173 (1988).
[2] I. Martinson, J. Opt. Soc. Am. B **5**, 2159 (1988).
[3] R. Hutton, Phys. Scr. **T73**, 25 (1997).
[4] K.-N. Huang, At. Data Nucl. Data Tables **32**, 504 (1985).
[5] W. R. Johnson, D. R. Plante, and J. Sapirstein, Adv. At., Mol., Opt. Phys. **35**, 255 (1995).
[6] U. I. Safronova, W. R. Johnson, and A. E. Livingston, Phys. Rev. A **60**, 996 (1999).
[7] E. N. Avgoustoglou and D. R. Beck, Phys. Rev. A **57**, 4286 (1998).
[8] D. R. Beck, Phys. Rev. A **57**, 4240 (1998).
[9] M. J. Vilkas, Y. Ishikawa, and K. Koc, Phys. Rev. A **60**, 2808 (1999).
[10] M. J. Vilkas, Y. Ishikawa, and K. Koc, Phys. Rev. E **58**, 5096 (1998).
[11] V. Kaufman and J. Sugar, J. Phys. Chem. Ref. Data **15**, 321 (1986).
[12] E. Träbert, S. B. Utter, and P. Beiersdorfer, Phys. Lett. A **272**, 86 (2000).
[13] F. G. Serpa, J. D. Gillaspy, and E. Träbert, J. Phys. B **31**, 3345 (1998).
[14] E. Träbert, P. Beiersdorfer, S. B. Utter, and J. R. Crespo López-Urrutia, Phys. Scr. **58**, 599 (1998).
[15] M. J. Vilkas, K. Koc, and Y. Ishikawa, Chem. Phys. Lett. **296**, 68 (1998).
[16] J. Sucher, Phys. Rev. A **22**, 348 (1980).
[17] M. H. Mittleman, Phys. Rev. A **24**, 1167 (1981).
[18] Y. Ishikawa and K. Koc, Phys. Rev. A **50**, 4733 (1994).
[19] K. Hirao, Chem. Phys. Lett. **190**, 374 (1992).
[20] K. Hirao, Chem. Phys. Lett. **201**, 59 (1993).
[21] C. Møller and M. S. Plesset, Phys. Rev. **46**, 618 (1934).
[22] P. Indelicato, O. Gorceix, and J. P. Desclaux, J. Phys. B **20**, 651 (1987).
[23] Y.-K. Kim, in *Atomic Processes in Plasmas, Gaithersburg, MD, 1989*, edited by Y.-K. Kim and R. C. E. Hon, AIP Conf. Proc. No. 206 (AIP, New York, 1990), p. 19.
[24] P. J. Mohr and Y. K. Kim, Phys. Rev. A **45**, 2727 (1992).
[25] A. I. Akhiezer and S. A. Berestetskii, *Quantum Electrodynamics* (Wiley Interstate, New York, 1965).
[26] I. P. Grant, J. Phys. B **7**, 1458 (1974).
[27] Y. Ishikawa and H. M. Quiney, Int. J. Quantum Chem., Symp. **21**, 523 (1987).
[28] A. W. Weiss and Y.-K. Kim, Phys. Rev. A **51**, 4487 (1995).
[29] J. R. Fuhr, W. C. Martin, A. Musgrove, J. Sugar, and W. L. Wiese, NIST Atomic Spectroscopic Database, available at http: //physics.nist.gov /PhysRefData /contents.html.
[30] C. Kohstall, S. Fritzsche, B. Fricke, and W.-D. Sepp, At. Data Nucl. Data Tables **70**, 63 (1998).